Stochastic motion of finite-size immiscible impurities in a dilute quantum fluid at finite temperature

Umberto Giuriato [*] and Giorgio Krstulovic

Université Côte d'Azur, Observatoire de la Côte d'Azur, CNRS, Laboratoire Lagrange, Boulevard de l'Observatoire CS 34229 - F 06304 NICE Cedex 4, France

The dynamics of an active, finite-size, and immiscible impurity in a dilute quantum fluid at finite temperature is characterized by means of numerical simulations of the Fourier truncated Gross-Pitaevskii equation. The impurity is modeled as a localized repulsive potential and described with classical degrees of freedom. It is shown that impurities of different sizes thermalize with the fluid and undergo a stochastic dynamics compatible with an Ornstein-Uhlenbeck process at sufficiently large time lags. The velocity correlation function and the displacement of the impurity are measured and an increment of the friction with temperature is observed. Such behavior is phenomenologically explained in a scenario where the impurity exchanges momentum with a dilute gas of thermal excitations, experiencing an Epstein drag.

I. INTRODUCTION

A Bose-Einstein condensate (BEC) is an exotic state of matter, which takes place in bosonic systems below a critical temperature, when a macroscopic fraction of particles occupy the same fundamental quantum state [1]. Almost three decades ago, Bose-Einstein condensation was observed for the first time by Anderson *et al.* in a dilute ultracold atomic gas [2]. Since then, BECs have been realized in a wide range of different systems, from solid-state quasiparticles [3,4] to light in optical microcavities [5].

Bose-Einstein condensation is intimately related to the notion of superfluidity, which is the capability of a system to flow without viscous dissipation [1]. Superfluidity was first detected almost one century ago in liquid helium ^{4}He [6,7] below 2.17 K, and it is a known feature also of atomic BECs and light in nonlinear optical systems [8]. Both superfluidity and Bose-Einstein condensation are a manifestation of quantum effects on a macroscopic scale, which is why these systems are usually called quantum fluids. Theoretically, a quantum fluid can be described by a macroscopic complex wave function. This represents the order parameter of the Bose-Einstein condensation phase transition and it is directly related to the density and the inviscid velocity of the superflow via a Madelung transformation [9].

As a consequence of superfluidity, an impurity immersed in a quantum fluid does not experience any drag and can move without resistance. However, if the speed of the impurity is too large, superfluidity is broken because of the emission of topological defects of the order parameter, known as quantum vortices [10–13]. Moreover, at finite temperature the thermal excitations in the system may interact with the impurities and drive their motion [14]. The behavior of particles and impurities immersed in a superfluid has been a central subject of study since long time [10]. The interest has been recently renewed by the experimental implementation of solidified hydrogen particles to visualize quantum vortices in superfluid helium [15,16], the study of polarons in atomic gases [17,18], and the use of impurities to investigate the properties of superfluids of light [19,20]. A particularly interesting kind of impurity arises in the immiscible regime of the multicomponent BEC. It has been shown that when two condensates of different species highly repel each other, one of the two components exists in a localized region and can be thought as a finite-size impurity [21,22]. If many components are present simultaneously, different phases can be identified, depending on the ratios between the coupling constants [22]. In particular, for positive scattering lengths between the impurity fields, the components separate from the main condensate and show a hard-sphere repulsion between each other. Experimentally, mixtures of different condensates have been realized with cold atomic gases [23,24], and the immiscibility properties have been studied [25].

In this work we aim at studying numerically the dynamics of an immiscible and finite-size impurity in a quantum fluid at finite temperature. There are several models which have been proposed to take into account finite-temperature effects in a quantum fluid, although at the moment there is no uniform consensus on which is the best one [26]. A successful example is the Zaremba-Nikuni-Griffin framework, in which a modified-dissipative Gross-Piteaevskii equation for the condensate wave function is coupled with a Boltzmann equation for the thermal cloud [27]. A simpler model is the Fourier truncated Gross-Pitaevskii (FTGP) equation, in which thermal fluctuations of the bosonic field are naturally taken into account without the coupling with an external thermal bath [28]. The main idea behind the FTGP model is that imposing an ultraviolet cutoff k_{max}, and truncating the system in Fourier space, allows for the regularization of the classical ultraviolet divergence and states at thermal equilibrium can be generated. The FTGP model has been successfully used to reproduce the condensation transition [28–31], to study finite-temperature effects on quantum vortex dynam-

*umberto.giuriato7@gmail.com

ics [32–34], and to investigate the effective viscosity in the system [35].

In this paper, we couple the FTGP equation with a minimal model for impurities, which are described as localized repulsive potentials with classical degrees of freedom [13,36]. It has been recently utilized systematically to investigate the interaction between particles and quantum vortices at very low temperature [37–40]. We stress that this minimal model is suitable for extensive numerical simulations and Monte Carlo sampling. Indeed, its simplicity makes it computationally much cheaper than more complex approaches in which the impurities have many (infinite) degrees of freedom, like the Gross-Clark model [41,42] or the multicomponent BEC model [22].

Recently, a drag force acting on an impurity in the weak coupling regime has been detected using a damped GP equation at finite temperature [43], extending an analytical work in which the resistance of the GP fluid on a point particle was studied at zero temperature [44]. In the case of immiscible active impurities, it has been shown that a multitude of them coupled with the FTGP model can form clusters, depending on the temperature and the ratio between the fluid-mediated attraction and the impurity-impurity repulsion [14]. Moreover, the presence of such clusters turned out to be responsible for an increase of the condensation temperature. However, the precise characterization of the dynamics of a single impurity immersed in a bath of FTGP thermal modes has not been addressed yet. This is indeed the purpose of this work. In the next section, we present the FTGP model coupled with a single three-dimensional impurity, and provide details for the numerical techniques used to simulate such system. In Sec. III, we present a statistical analysis of extensive numerical simulations of the system. In particular, we find that at large times the dynamics of an impurity in a finite-temperature quantum fluid is akin to an Ornstein-Uhlenbeck process with a temperature-dependent friction coefficient, that we are able to explain. Eventually, we exploit this information to show that for the sizes of the impurities considered, their motion is consistent with a scenario where the thermal excitations behave as a gas of waves rather than a continuum liquid.

II. FINITE-TEMPERATURE MODEL

We use the Fourier truncated Gross-Pitaevskii model to describe a weakly interacting quantum fluid at finite temperature, with a repulsive impurity immersed in it [14]. The Hamiltonian of the model is given by

$$
H = \int \left(\frac{\hbar^2}{2m} |\nabla \psi|^2 + \frac{g}{2} |\mathcal{P}_G[|\psi|^2]|^2 \right) dx
$$
$$
+ \int V_I(|\mathbf{x} - \mathbf{q}|) \mathcal{P}_G[|\psi|^2] \, dx + \frac{\mathbf{p}^2}{2M_I}, \quad (1)
$$

where $\psi(\mathbf{x}, t)$ is the bosonic field, m is the mass of the constituting bosons, and $g = 4\pi a_s \hbar^2/m$ is the self-interaction coupling constant, with a_s the boson s-wave scattering length.

The bosonic field is coupled with an impurity of mass M_I, described by its classical position $\mathbf{q}(t)$ and momentum $\mathbf{p}(t) = M_I \dot{\mathbf{q}}(t)$. The impurity is modeled by a repulsive potential $V_I(|\mathbf{x} - \mathbf{q}|)$, which defines a spherical region centered in $\mathbf{q}(t)$

where the condensate is completely depleted. Note that the functional shape of the potential $V_I(|\mathbf{x} - \mathbf{q}|)$ is not important, provided that it is sufficiently repulsive to completely deplete the fluid. The relevant parameter is indeed the size of the depleted region, which in turns identifies the impurity radius a_I. The Galerkin projector $\mathcal{P}_G$ truncates the system imposing an UV cutoff in Fourier space: $\mathcal{P}_G[\hat{\psi}_{\mathbf{k}}] = \theta(k_{max} - |\mathbf{k}|)\hat{\psi}_{\mathbf{k}}$ with $\theta(\cdot)$ the Heaviside theta function, $\hat{\psi}_{\mathbf{k}}$ the Fourier transform of $\psi(\mathbf{x})$ and $\mathbf{k}$ the wave vector. The time-evolution equation of the wave function and the impurity are obtained straightforwardly by varying the Hamiltonian (1):

$$
i\hbar \frac{\partial \psi}{\partial t} = \mathcal{P}_G\left[-\frac{\hbar^2}{2m}\nabla^2\psi + g\mathcal{P}_G[|\psi|^2]\psi + V_I(|\mathbf{x} - \mathbf{q}|)\psi \right],
$$
(2)

$$
M_I \frac{d\dot{\mathbf{q}}}{dt} = -\int V_I(|\mathbf{x} - \mathbf{q}|)\mathcal{P}_G[\nabla|\psi|^2] \, dx. \quad (3)
$$

Note that the projection of the density $|\psi|^2$ in Eq. (2) is a dealiasing step that is necessary to conserve momentum [34] in the truncated equations. This procedure slightly differs with the projected Gross-Pitaevskii model [28] as some high-momentum scattering processes are not considered in the FTGP framework.

At zero temperature and without the impurity, Eq. (2) can be linearized about the condensate ground state $\psi_0 = |\psi_0| \exp(-i\mu t/\hbar)$, fixed by the chemical potential $\mu = g|\psi_0|^2$. The excitations of the condensate propagate with the Bogoliubov dispersion relation

$$
\omega_B(k) = ck\sqrt{1 + \frac{\xi^2 k^2}{2}}, \quad (4)
$$

where $k = |\mathbf{k}|$, $c = \sqrt{g|\psi_0|^2/m}$ is the speed of sound, and $\xi = \sqrt{\hbar/2gm|\psi_0|^2}$ defines the healing length at zero temperature. Note that the impurity completely depletes the condensate in the region where $V_I > \mu$.

The Hamiltonian H and the number of bosons $N = \int |\psi|^2 dx$ are invariants of the FTGP model. Thus, it possesses finite-temperature absolute equilibrium solutions, distributed with the probability

$$
\mathbb{P}[\psi, \mathbf{q}, \dot{\mathbf{q}}] \propto e^{-\beta(H - \mu N)}. \quad (5)
$$

The concept of absolute equilibria of Fourier truncated equations was first introduced in the context of the Euler equation [45,46] and directly generalizes to FTGP [34]. Such equilibria are steady solutions of the associated Liouville equation. The Liouville equation describes the microcanonical evolution of the phase-space distribution function of an ensemble of states driven by Eqs. (2) and (3). Note that a state which solves Eqs. (2) and (3) conserves the invariants N and H, and the equilibrium distribution in Eq. (5) is nothing but the probability of picking one of these states at given inverse temperature β and chemical potential μ. This is true whether the impurity is present in the system or not. The argument of the exponential in Eq. (5) is a linear combination of the invariants H and N, and β is a Lagrange multiplier identified with the inverse temperature. Given a random initial condition with energy H and number of bosons N, long time integration of Eqs. (2) and (3) will let the system evolve to an equilibrium

state belonging to the distribution (5). The temperature is not directly available as a control parameter since such dynamics is microcanonical, but it is biunivocally associated to the given conserved invariants [28].

At finite temperature, many modes are excited and interact nonlinearly. Such interactions lead to a spectral broadening of the dispersion relation, together with small corrections of the frequency. Overall, the dispersion relation can be well approximated taking into account the depletion of the condensate mode in the following manner [35]:

$$\omega_B^T(k) = ck\sqrt{n_0(T) + \frac{\xi^2 k^2}{2}}, \qquad (6)$$

where $n_0(T)$ is the condensate fraction. We define it as

$$n_0(T) = \frac{\langle |\int \psi \, d\mathbf{x}|^2 \rangle_T}{\langle |\int \psi \, d\mathbf{x}|^2 \rangle_{T=0}}, \qquad (7)$$

namely, as the ratio between the occupation number of the zero mode at temperature T and at temperature $T = 0$. With such definition, the condensate fraction is normalized to be one at zero temperature. In this way, the depletion of the condensate due to the presence of the impurity is properly taken into account [14]. The fraction of superfluid component $n_s(T) = \rho_s / \bar{\rho}$ and normal fluid component $n_n(T) = \rho_n / \bar{\rho}$, where $\bar{\rho} = \frac{1}{L^3} \int m |\psi|^2 \, d\mathbf{x}$ is the average mass density, can be computed using a linear response approach [14,47,48]. They read as, respectively,

$$n_n(T) = \frac{\lim_{k \to 0} \chi_I(k)}{\lim_{k \to 0} \chi_C(k)}, \quad n_s(T) = 1 - n_n(T), \qquad (8)$$

where $\chi_C(k)$ and $\chi_I(k)$ are, respectively, the compressible (longitudinal) and incompressible (transverse) coefficients of the two-point momentum correlator:

$$\langle \hat{j}_i(\mathbf{k}) \hat{j}_j(-\mathbf{k}) \rangle \propto \frac{k_i k_j}{k^2} \chi_C(k) + \left(\delta_{ij} - \frac{k_i k_j}{k^2} \right) \chi_I(k), \qquad (9)$$

with $\hat{j}_i(\mathbf{k}, t)$ the Fourier transform of the ith component of the momentum density $j_i(\mathbf{x}, t) = \frac{i\hbar}{2} [\psi \partial_i \psi^* - \psi^* \partial_i \psi]$.

A. Numerical methods and parameters

In the numerics presented in this work, we integrate the system (2) and (3) by using a pseudospectral method with $N_{res} = 128$ uniform grid points per direction of a cubic domain of size $L = 2\pi$. We further set the UV cutoff $k_{max} = N_{res}/3$, so that, aside from the Hamiltonian H and the number of bosons N, the truncated system (2) and (3) conserves the total momentum $\mathbf{P} = \int \frac{i\hbar}{2} (\psi \nabla \psi^* - \psi^* \nabla \psi) d\mathbf{x} + \mathbf{p}$ as well (provided that initially $\mathcal{P}_G[\psi] = \psi$ and $\mathcal{P}_G[V_I] = V_I$) [34,39]. In thermal states, the cutoff k_{max} plays an important role. The dimensionless parameter ξk_{max} controls the amount of dispersion of the system and therefore the strength of the nonlinear interactions of the BEC gas. The smaller its value, the stronger the interaction is. Note that, as scales of the order of the healing length have to be resolved numerically, it cannot be arbitrarily small. See, for instance, Refs. [34,35] for further discussions. In this work we fix this parameter to $\xi k_{max} = 2\pi/3$. Note that in our results all the lengths are expressed in units of the healing length at zero temperature
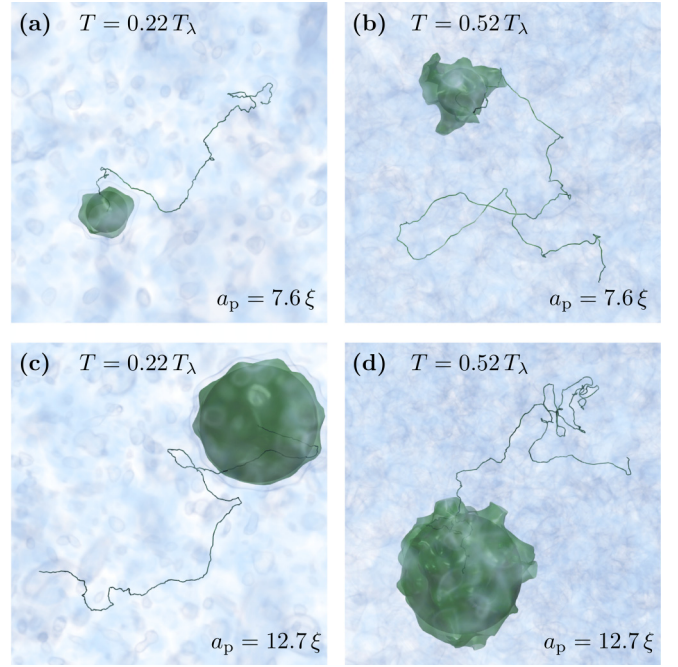

FIG. 1. Snapshots of the GP field with an impurity of size $a_I = 7.6\xi$ at time $t = 3056\xi/c$ [(a), (b)] and an impurity of size $a_I = 12.7\xi$ at time $t = 7130\xi/c$ [(c), (d)] at temperatures $T = 0.22 T_\lambda$ [(a), (c)] and $T = 0.52 T_\lambda$ [(b), (d)]. The GP sound waves are rendered in blue, the dark sphere is the impurity potential, and the green surfaces are contours of the GP density at $\rho/\bar{\rho} = 0.15$. The impurity trajectory is displayed as a solid line.

ξ and the velocities in units of the speed of sound c at zero temperature. In these units, the system size is $L = 128\xi$.

The potential used to model the impurity is a smoothed hat function $V_I(r) = \frac{V_0}{2} (1 - \tanh [\frac{r^2 - \eta_a^2}{4\Delta_a^2}])$. The impurity radius a_I is estimated at zero temperature by measuring the volume of the displaced fluid $\frac{4}{3}\pi a_I^3 = \int (|\psi_0|^2 - |\psi_p|^2) \, d\mathbf{x}$, where ψ_p is the steady state with one impurity. The impurity mass density is then $\rho_I = M_I / (\frac{4}{3}\pi a_I^3)$. In all the simulations we fix $\mu = |\psi_0| = 1$ and for the impurity potential $V_0 = 20\mu$ and $\Delta_a = 2.5\xi$. We consider an impurity of radius $a_I = 7.6\xi$ setting $\eta_a = 2\xi$ and an impurity of size $a_I = 12.7\xi$ setting $\eta_a = 10\xi$.

Note that, although the shape of the impurity potential is fixed, fluctuations of the impurity surface are allowed by the model. Such fluctuations are shown in Fig. 1 (that will be commented in Sec. III) as green contours of the fluid density at a low value around the spherical potential.

We prepare separately the ground state with an impurity ψ_p (at zero temperature) and the FTGP states at finite temperature ψ_T, without the impurity. The first one is obtained by performing the imaginary-time evolution of Eq. (2), while the second one is realized with the stochastic real Ginzburg-Landau (SRGL) [14,34,35], protocol that allows to explicitly control the temperature. The SRGL method is briefly recalled below. The initial condition for the FTGP simulations is then obtained as $\psi = \psi_p \times \psi_T$. For our analysis, we considered ~ 22 different realizations for each of the 15 studied temperatures and for each impurity. The initial velocity of the

impurity is always set to zero and the temporal length of each realization is $\sim 9000\,\xi/c$. In all the statistical analysis presented in the following sections, we checked that including or not the data associated to the early times of the simulation does not change the results. The thermalization of the impurity will be studied explicitly in Sec. III, but this fact gives already a first indication that the impurity reaches the equilibrium with the thermal bath in the very early stages of the simulations.

We operatively define the condensation temperature T_λ as the first point of the temperature scan at which the condensate fraction $n_0(T)$ goes to zero. The normal fluid fraction $n_n(T)$ and consequently the superfluid fraction $n_s(T) = 1 - n_n(T)$ are evaluated numerically with the following protocol [48]. At fixed temperature, we measure the angle-averaged incompressible and compressible spectra of the momentum correlator, respectively, $\chi_I^{1d}(k) \propto \langle k^2 |\mathbf{j}_I(\mathbf{k})|^2 \rangle$ and $\chi_C^{1d}(k) \propto \langle k^2 |\mathbf{j}_C(\mathbf{k})|^2 \rangle$. We fit the logarithm of $\chi_I^{1d}(k)/k^2$ and $\chi_C^{1d}(k)/k^2$ with a cubic polynomial in the range $3L/2\pi < k < 3k_{max}/2$; we extrapolate the values of the fits at $k = 0$ and finally divide them to get $n_n(T) = \chi_I(k=0)/\chi_C(k=0)$. Such method works well at low temperatures while it is strongly affected by numerical noise at temperatures $T \gtrsim T_\lambda$ [48]. These last points are then simply assumed to be equal to zero.

Finally, note that in this work, if not explicitly specified, all the averages are intended over realizations for a fixed temperature T. Moreover, because of isotropy, we treat each dimension of any vectorial quantity as a different realization of the same distribution.

B. Grand-canonical thermal states

We recall here the SRGL protocol used to obtain equilibrium thermal states of the truncated GP equation. We refer to Ref. [34] for further details about the method. The FTGP grand-canonical thermal states obey the (steady) Gibbs distribution which coincides with Eq. (5). A stochastic process that converges to a realization of this probability distribution is given by the following stochastic equation (in physical space):

$$\hbar \frac{\partial \psi}{\partial t} = \mathcal{P}_G \left[\frac{\hbar^2}{2m} \nabla^2 \psi + \mu\psi - g\mathcal{P}_G[|\psi|^2]\psi + V_I(|\mathbf{x} - \mathbf{q}|)\psi \right]$$
$$+ \sqrt{\frac{2\hbar}{\beta L^3}} \mathcal{P}_G[\zeta(\mathbf{x}, t)], \qquad (10)$$

where $\zeta(\mathbf{x}, t)$ is a complex Gaussian white noise with zero mean and delta correlated in space and time: $\langle \zeta(\mathbf{x}, t)\zeta^*(\mathbf{x}', t') \rangle = \delta(\mathbf{x} - \mathbf{x}')\delta(t - t')$. In principle, such process is coupled with analogous equations for the impurity degrees of freedom [14]. Here, we do not consider them since we are interested in generating thermal states without impurities. As explained in the previous section, the impurity is added afterwards to the thermal states in order to observe its dynamics according to the evolution equations (2) and (3). In the right-hand side of Eq. (10) a deterministic term and a stochastic term compete against each other. The distribution which entails the balance between such fluctuations and dissipation is Eq. (5), i.e., the steady solution of the Fokker-Planck equation associated to Eq. (10) [34].

We define the temperature as $T = 1/k_\mathcal{N}\beta$, where $k_\mathcal{N} = L^3/\mathcal{N}$ and $\mathcal{N} = \frac{4}{3}\pi k_{max}^3$ is the number of Fourier modes in

the system. With this choice, the temperature has units of energy density and the intensive quantities remain constant in the thermodynamic limit, that is $k_{max} \to \infty$ with L constant. Finally, in order to control the steady value of the average density $\bar{\rho}$, the chemical potential is also dynamically evolved with the *ad hoc* equation $\dot{\mu} = -\nu_\rho(\bar{\rho} - \bar{\rho}_t)$ during the stochastic relaxation. In this way, the system converges to the control density $\bar{\rho} = \bar{\rho}_t$ that we set equal to $m|\psi_0|^2 = 1$.

We finally mention that a similar approach can be used to generate and study thermal states, which is the stochastic GP model [26]. There, the stochastic relaxation (10) is combined with the physical GP evolution (2). However, unlike the FTGP model, the stochastic GP model is dissipative and has an adjustable parameter in which the interaction between the condensate and the thermal cloud is encoded.

III. IMPURITY MOTION

We perform a series of numerical simulations of the models (2) and (3), varying the temperature and the size of the impurity. Typical impurity trajectories are displayed in Fig. 1 for two different temperatures, together with a volume rendering of the field and of the impurity. The motion of the impurity is clearly driven by a random force, due to the interaction with the thermal excitations of the condensate.

Before studying the stochastic dynamics of the impurity, we characterize some properties of the thermal states that will be used later. In Fig. 2(a) we show the condensate fraction n_0, the superfluid component n_s, and the normal fluid component n_n plotted against temperature. The lines refer to the simulations without impurity while the circles are obtained in presence of the largest impurity considered ($a_I = 12.7\xi$). Almost no difference between the two cases is detected since the volume occupied by the impurity is only 0.5%. Indeed, in Ref. [14] it was shown that the condensate fraction starts to increase at high temperatures if the impurities filling fraction is larger than 4%. We can therefore safely assume that the impurity has no impact on the statistical properties of the thermal fluctuations.

From the impurity (3), we observe that the quantum fluid interacts with the impurity via a convolution between the impurity potential and the density gradient. It is thus interesting to understand the typical correlation time of density fluctuations, in particular of its gradients. In Fig. 2(b) we compute the decorrelation time τ_{GP} of the thermal excitations as a function of temperature. Such time is evaluated performing a FTGP evolution of thermal states without impurity and considering the time correlator of one of the components of the density gradient:

$$C_{\partial\rho}(t) = \frac{\langle \partial_i\rho(t_0)\partial_i\rho(t_0 + t) \rangle}{\langle (\partial_i\rho)^2 \rangle}. \qquad (11)$$

The averages in Eq. (11) are performed over space and different realizations. Three examples for three different temperatures of the time evolution of this correlator are shown in the inset of Fig. 2(b). They show a damped oscillating behavior and touch zero for the first time after a time $\sim 1c/\xi$. We estimate the decorrelation time τ_{GP} as the time after which the correlator (11) is always less than 1%. At timescales larger than τ_{GP}, we expect that the interactions between the impurity
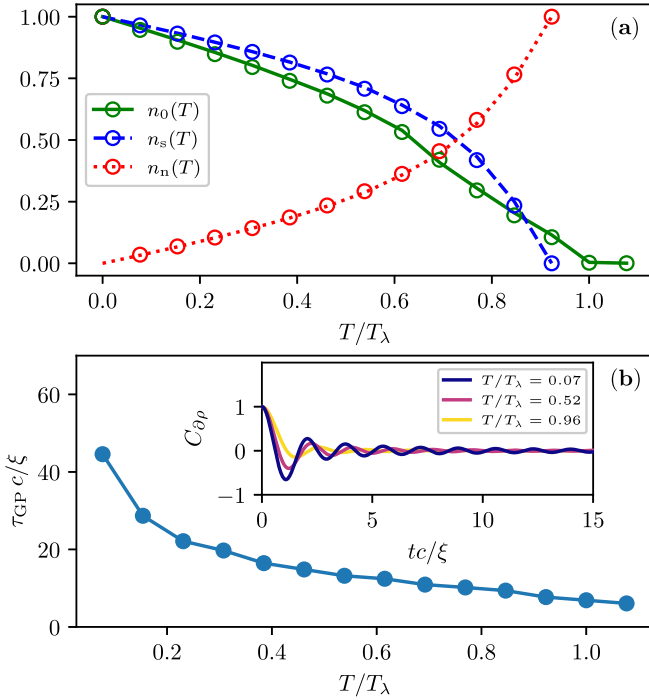
FIG. 2. (a) Temperature evolution of condensate fraction (green solid line), superfluid fraction (dashed blue line), and normal fraction (dotted red line) for simulations without impurity. The circles of corresponding colors refer to simulations in presence of an impurity of size $a_I = 12.7\xi$ and mass density $\rho_I = \bar{\rho}$. (b) Temperature evolution of the decorrelation time of the FTGP density gradients. (Inset) Time evolution of the two-point correlators of the FTGP density gradients (11) for three different temperatures.

and the thermal excitations can be considered as random and rapid. Before checking if this is the case, we verify explicitly whether the impurity reaches the thermal equilibrium with the quantum fluid.

If the number of the excitations-impurity interactions is large, the velocity of the impurity is expected to be normally distributed at the equilibrium, in accordance with the central limit theorem. Indeed, we show this in Fig. 3, where the probability density function (PDF) for the single component of the impurity velocity is displayed. Assuming ergodicity, the PDFs are computed averaging also over time, besides over realizations. Since we expect the impurity to be in thermal equilibrium with the surrounding GP fluid, the second-order moment of its velocity should relax to a constant value, that is related to the temperature via the equipartition of energy:

$$\langle \dot{q}_i^2 \rangle = \frac{k_\mathcal{N} T}{M_I}. \qquad (12)$$

The perfect agreement between Eq. (12) and the numerical simulations is displayed in Fig. 4. It confirms that the impurity is indeed in thermal equilibrium with the thermal bath. Note that the linear scaling with temperature persists also at high temperatures, where the GP energies are not in equipartition anymore because of high nonlinear interactions. This is not a contradiction since the impurity is a classical object with a simple quadratic kinetic energy. For comparison, the deviation from equipartition of the GP energy density $e_{GP} =$
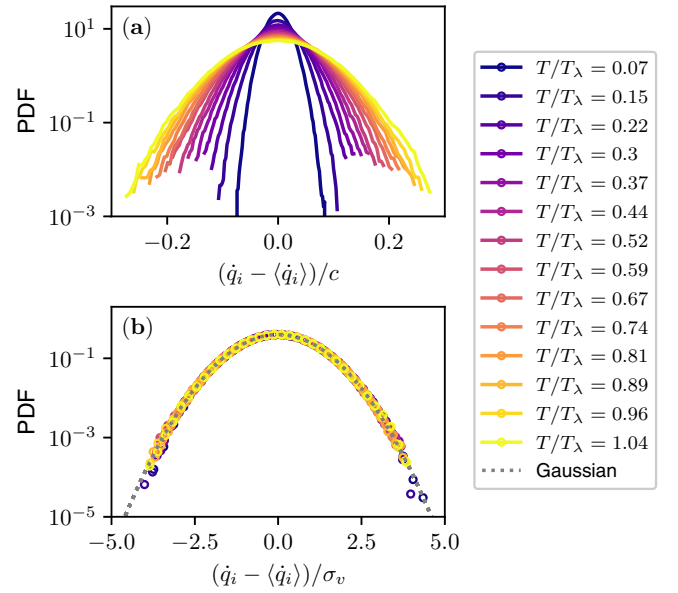

FIG. 3. PDF of the single-component velocity of an impurity of size $a_I = 7.6\xi$ and mass density $\rho_I = \bar{\rho}$, for different temperatures. (a) Velocities normalized with the speed of sound at zero temperature. (b) Velocities normalized with the standard deviation. Dotted black line is a Gaussian distribution with zero mean and unit variance.

$(H - \mu N)/L^3 + \mu^2/2g$ (without impurities) is reported in the inset of Fig. 4.

We consider now the evolution of the two-point impurity velocity correlator $C_v(t)$. If the collisions between the superfluid thermal excitations and the impurity are fast and random, we expect it to decay as

$$C_v(t) = \lim_{t \to \infty} \frac{\langle \dot{q}_i(t_0)\dot{q}_i(t_0 + t) \rangle - \langle \dot{q}_i \rangle^2}{\langle \dot{q}_i^2 \rangle - \langle \dot{q}_i \rangle^2} = e^{-\frac{t}{\tau_I}}, \qquad (13)$$

where τ_I is the dynamical correlation time of the impurity velocity. Specifically, the behavior (13) should certainly hold
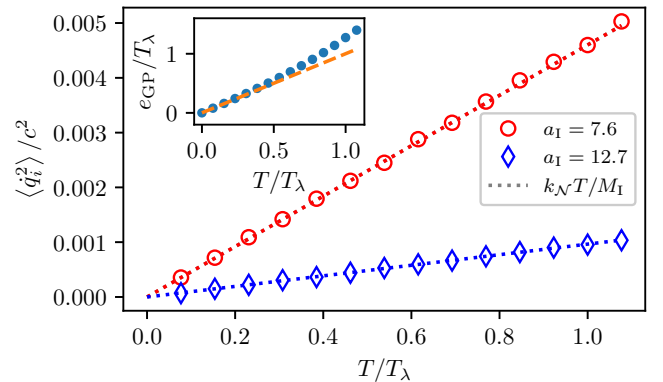

FIG. 4. Second-order moment of the single-component velocity of impurities of size $a_I = 7.6\xi$ (red circles) and $a_I = 12.7\xi$ (blue diamonds), as a function of the temperature. The mass density is $\rho_I = \bar{\rho}$ for both. (Inset) GP energy density versus temperature (blue points). Orange dashed line is the equipartition line $e_{GP} = T_\lambda$.
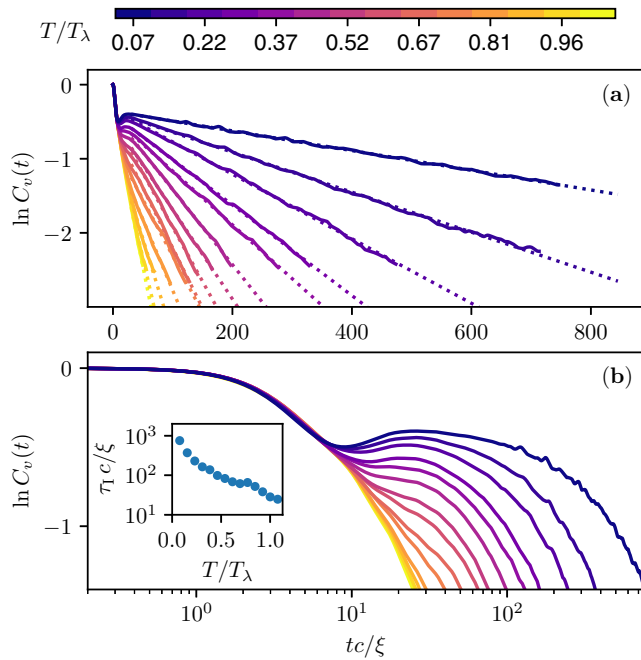
FIG. 5. Time evolution of the two-point velocity correlator for the impurity of size $a_I = 7.6\xi$ and mass density $\rho_I = \bar{\rho}$ in (a) log-lin scale and (b) log-log scale. Different colors are associated to different temperatures (same legend of Fig. 3). Dotted lines are linear fits. (Inset) Temperature evolution of the dynamical correlation time of the impurity.

at time lags larger than the decorrelation time of the GP excitations τ_{GP}, estimated in Fig. 2(b). This scenario is confirmed by the measurements of $C_v(t)$, reported in Fig. 5 for the impurity of size $a_I = 7.6\xi$. The exponential decay is evident for time lags larger than $\sim 10\xi/c$ for all the temperatures.

According to the results mentioned so far, at sufficiently large timescales the interactions between the impurity and the thermal bath can be considered to be effectively fast, random, and decorrelated. Thus, it is natural to suppose that the impurity dynamics may be described by the Ornstein-Uhlenbeck (OU) process [49]:

$$M_I \ddot{\mathbf{q}} = -\gamma \dot{\mathbf{q}} + \sqrt{\sigma^2} \zeta_r(t), \tag{14}$$

where $\zeta_r(t)$ is a (Gaussian) white noise in time, i.e., $\langle \zeta_r(t) \rangle = 0$ and $\langle \zeta_{r,i}(t_1) \zeta_{r,j}(t_2) \rangle = \delta_{ij} \delta(t_1 - t_2)$ where σ^2 is related to the diffusion coefficient. The term $-\gamma \dot{\mathbf{q}}$ is the drag force, with γ a friction coefficient that in general may depend on temperature and on the impurity size. In particular, the friction should be directly related to exponential decay timescale τ_I of the correlator (13) as $\gamma = M_I/\tau_I$. In Fig. 5 we clearly see that the correlators decay faster for higher temperatures. The values of the correlation time τ_I at different temperatures are obtained through linear fits of $\ln C_v(t)$, shown as dotted lines in Fig. 5(a). The decreasing of τ_I with temperature is then explicitly displayed in the inset of Fig. 5(b). Note that $\tau_I \gg \tau_{GP}$, consistently with the assumptions of the OU process. The physical consequence of such behavior, according to the OU picture, is that the friction γ between the impurity and the fluid is larger for larger temperatures. We will dedicate the

next section to the discussion on the temperature dependence of γ.

We briefly comment on the short time-lag limit ($t \lesssim 10\xi/c$), where the measured correlator appears to decay fast and with the same slope for all the temperatures. This is particularly evident in the log-log plots in Fig. 5(b). In this regime, the assumptions necessary for an OU regime to be established are certainly not valid. Indeed, we are looking at timescales shorter than the decorrelation time of the thermal excitations τ_{GP}, so that the collisions between the excitations and the impurity cannot be considered random, rapid, and decorrelated as in the forcing $\zeta_r(t)$ in (14). It is worth noting that, for low temperatures, the velocity correlator partially recovers before the exponential decay. This unusual feature may be a consequence of a lack of decorrelation due to the small fraction of thermal excitations at low temperatures, which prevents the emergence of a diffusive regime. Such phenomenon requires further investigations.

Another important prediction that can be obtained from the OU process is that the variance of the displacement $\delta_t q_i(t) = q_i(t + t_0) - q_i(t_0)$ obeys the law

$$\langle (\delta_t q_i)^2 \rangle = \frac{\sigma^2 M_I}{\gamma^3} \left(\frac{\gamma}{M_I} t - 1 + e^{-\frac{\gamma}{M_I} t} \right). \tag{15}$$

Two regimes can be identified. At short time lags [but still large enough to consider the forcing $\zeta_r(t)$ delta correlated], the displacement is ballistic

$$\langle (\delta_t q_i)^2 \rangle \xrightarrow[t \ll M_I/\gamma]{} \frac{\sigma^2}{2\gamma M_I} t^2. \tag{16}$$

Conversely, after the dynamical relaxation, a diffusive regime is established

$$\langle (\delta_t q_i)^2 \rangle \xrightarrow[t \gg M_p/\gamma]{} \frac{\sigma^2}{\gamma^2} t = 2Dt, \tag{17}$$

where we have defined the diffusion constant $D = \sigma^2/2\gamma^2$.

Finally recall that, since in the OU process we also have that $\langle \dot{q}_i^2 \rangle = \sigma^2/2M_I\gamma = D\gamma/M_I$, the diffusion coefficient in Eq. (17) can be related to the equipartition of energy in thermal equilibrium (5) through the Einstein relation

$$D = \frac{k_\mathcal{N} T}{\gamma}. \tag{18}$$

The measurements of the average squared displacement for the impurity of size $a_I = 7.6\xi$ are shown in Fig. 6 for all the temperatures analyzed, and compared with the OU predictions. Once the squared displacement is normalized with the prefactor of the prediction (15) and assuming the Einstein relation (18) to estimate the diffusion coefficient, the separation between the ballistic regime and the diffusive one is apparent (bottom panel). The transition happens at the measured values of the dynamical correlation time $t = \tau_I$, confirming the validity of the analysis of the velocity correlator. The diffusion coefficient D is measured as the slope of the squared displacement in the diffusive regime and it is shown in the inset of Fig. 6(a). It is slightly larger than the prediction given by the Einstein relation (18). Such trend can be the signature of a memory effect due to a stochastic forcing of the fluid on the impurity which is not perfectly
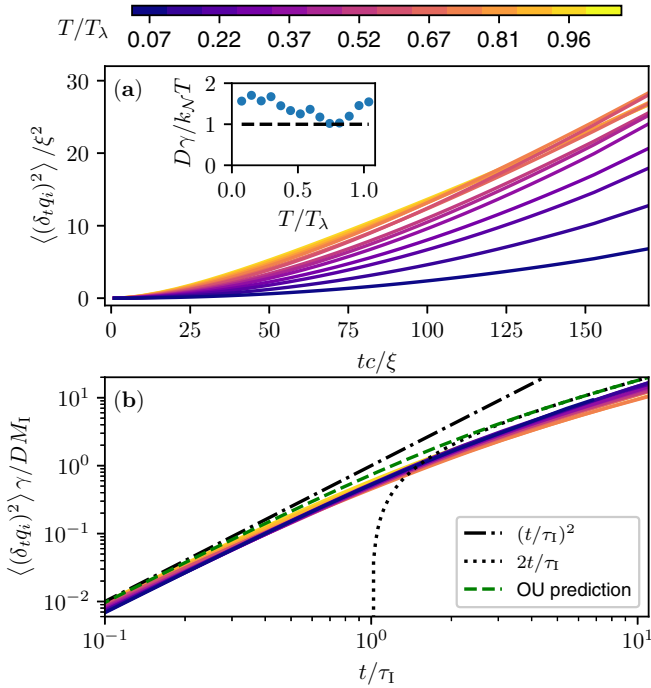
FIG. 6. Time evolution of the averaged squared displacement for the impurity of size $a_I = 7.6\xi$ for different temperatures. Different colors are associated to different temperatures (same legend of Fig. 3). Dashed green line is the prediction (15), assuming the Einstein relation (18), dashed-dotted black line and dotted line are, respectively, the asymptotic equations (16) and (17). (a) lin-lin scale, times normalized with ξ/c and distances normalized with ξ. (b) log-log scale, times normalized with the correlation time τ_I and distances normalized with the prefactor of (15). (Inset) Measured diffusion coefficient as a function of temperature compared with the Einstein relation (18).

delta correlated. For instance, it could be traced back to the presence of coherent structures in the fluid or to the impurity surface fluctuations, due to the actual interaction between the impurity and the thermal excitations.

Friction modeling

In this section we show explicitly the behavior of the friction coefficient observed in the numerical simulations and we give a phenomenological argument to explain it. In Fig. 7, the friction γ is plotted as a function of the temperature for the two impurity sizes analyzed (red circles for the small one and blue diamonds for the large one). Each value of $\gamma = M_p/\tau_I$ is estimated from the measured decay time τ_I of the impurity velocity correlator, shown in the inset of Fig. 5(b).

In general terms, the friction γ depends on the interaction between the impurity and the surrounding fluid. For a classical fluid there are different regimes, depending on the value of the Knudsen number $\mathrm{Kn} = \lambda_{\mathrm{mfp}}/a_I$, where λ_{mfp} is the mean-free path of the fundamental constituents of the fluid. If $\mathrm{Kn} \ll 1$, at the scale of the impurity, the fluid can be effectively considered as a continuous medium and the Navier-Stokes equations hold. As a consequence, the drag force acting on the impurity is the standard Stokes drag $\mathbf{F}_d = -6\pi a_I \eta \dot{\mathbf{q}}$ [50], so that the
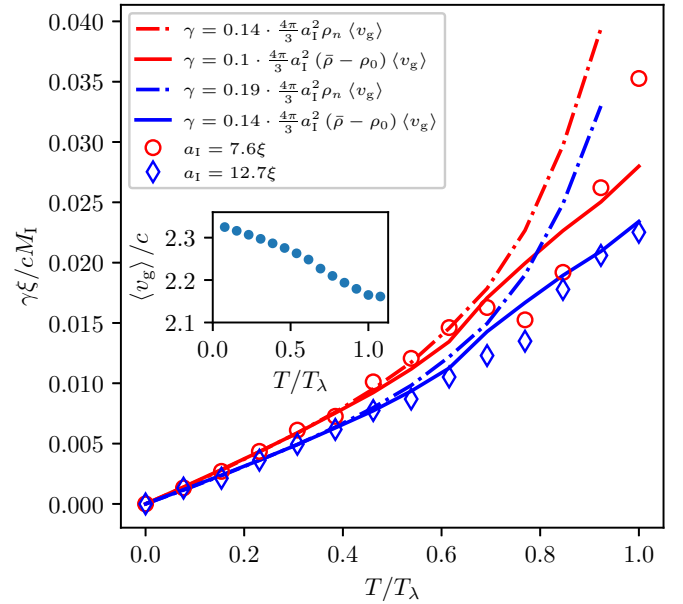

FIG. 7. Friction coefficient γ nondimensionalized by cM_I/ξ as a function of the temperature, for impurities of size $a_I = 7.6\xi$ (red circles) and $a_I = 12.7\xi$ (blue diamonds), with mass density $\rho_I = \bar{\rho}$. Dashed-dotted lines are fits of the Epstein drag (20) using the normal fluid density ρ_n. Solid lines are fits of the Epstein drag using the density of noncondensed modes $\bar{\rho} - \rho_0$. (Inset) Average excitation velocity $\langle v_g \rangle$ (21) as a function of temperature.

friction is related to the viscosity η as

$$\gamma = 6\pi a_I \eta. \tag{19}$$

Instead, if $\mathrm{Kn} \gg 1$, the fluid behaves as a dilute gas of free molecules. In this case, the resistance of the impurity is well described by the Epstein drag [51]:

$$\mathbf{F}_d = -\gamma \dot{\mathbf{q}}, \quad \gamma = \frac{4\pi}{3} C_d a_I^2 \rho_g \langle v_g \rangle = C_d \frac{M_I \rho_g \langle v_g \rangle}{a_I \rho_I}, \tag{20}$$

where ρ_g is the mass density of the gas and $\langle v_g \rangle \gg |\dot{\mathbf{q}}|$ is the average velocity of the molecules. The prefactor C_d is a dimensionless constant that depends on the interaction between the impurity and the fluid molecules. In the case of elastic collisions of the fluid excitations (specular reflection), a simple way of understanding the formula (20) is summarized in the following [52]. If an object of mass M_I moves with velocity $\dot{\mathbf{q}}$ in an isotropic gas of free molecules, the momentum exchanged in the collision between a surface element dA and a molecule (assuming elastic collisions) is $\Delta \mathbf{p} \sim -2m_g |\dot{\mathbf{q}}| \cos\theta \hat{\mathbf{n}}$, where $m_g \ll M_I$ is the molecule mass and θ is the angle between the object velocity and the outward normal to the surface element $\hat{\mathbf{n}}$. Assuming that the typical speed of the molecules $\langle v_g \rangle$ is much larger than the object velocity, the average number of collisions in a time interval Δt is $dn_{\mathrm{coll}} = n_g \langle v_g \rangle \Delta t \, dA$, which is the number density of molecules $n_g = \rho_g/m_g$ times the volume spanned by each molecule $\langle v_g \rangle \Delta t \, dA$. The infinitesimal force arising from the momentum exchange is therefore $d\mathbf{F}_d = (\Delta \mathbf{p}/\Delta t) \, dn_{\mathrm{coll}}$. By symmetry, if the object is spherical, the force components orthogonal to its direction of motion will cancel. Accounting for this, the net drag force results from the integration

of $|d\mathbf{F}_d| \cos\theta(\dot{\mathbf{q}}/|\dot{\mathbf{q}}|)$ over half of the sphere surface. This leads precisely to Eq. (20) with $C_d = 1$. Considering different reflection mechanisms leads to the same equation with a different value of the prefactor C_d. For instance, in the case of full accommodation of the excitations with the impurity surface one gets $C_d = (1 + \pi/8) \sim 1.39$ [51].

The mean-free path $\lambda_{\mathrm{mfp}}(T)$ in the FTGP model has been recently estimated in Ref. [35] as the product of the group velocity of the excitations and the nonlinear interaction time (i.e., the reciprocal of the spectral broadening of the dispersion relation) at a given temperature. For $\xi k_{\max} = 2\pi/3$, the value used in this work, the mean-free path λ_{mfp} turns out to lie between $10\,\xi$ and $50\,\xi$ at temperatures $T < 0.7\,T_\lambda$, thus larger than the sizes of the impurities studied here (cf. Fig. 14 of Ref. [35]). As a consequence, we can treat the fluid as a gas of free molecules and confront the measured friction with the Epstein drag. In particular, the role of "gas molecules" in the GP fluid is played by the thermal excitations. Therefore, we can substitute the gas density ρ_g in Eq. (20) with the density of the noncondensed modes $\rho_g = \bar{\rho} - \rho_0$, where $\rho_0 = n_0\bar{\rho}$ or with the normal fluid density $\rho_g = \rho_n = n_n\bar{\rho}$, computed using the momentum density correlator [48] (see Fig. 2). The velocity of the excitations $v_g = \frac{\partial \omega_k}{\partial k}$ is averaged as

$$\langle v_g \rangle = \frac{\sum_{|\mathbf{k}| \in S_\mathbf{k}} n_\mathbf{k} \frac{\partial \omega_k}{\partial k}}{\sum_{|\mathbf{k}| \in S_\mathbf{k}} n_\mathbf{k}} = \frac{\sum_{k=1}^{k_{\max}} k^2 n_k^{1d} \frac{\partial \omega_k}{\partial k}}{\sum_{k=1}^{k_{\max}} n_k^{1d}}, \qquad (21)$$

with $n_\mathbf{k}$ the occupation number of the mode $\mathbf{k} \in S_\mathbf{k} = \{1 \leqslant |\mathbf{k}| \leqslant k_{\max}\}$ and $n_k^{1d} = \sum_{|\mathbf{k}|=k} n_\mathbf{k}$ its angle average.

In Fig. 7, the Epstein drag prediction (20) is compared with the numerical data. Both using the normal fluid density (dashed-dotted lines) or the density of noncondensed modes (solid lines) we get a good accordance at low temperatures, with a fitted prefactor C_d, whose values are of the order 0.1. Note that in this way we are implicitly guessing that the impurity-excitations interaction is independent of temperature. The specific values of C_d are reported in the legend of Fig. 7. They are consistent with a reasonable scenario in which thermal waves are much less efficient in transferring momentum to the impurity with respect to the standard particles reflection mechanisms [51]. We observe that C_d is slightly increasing with the impurity size (perhaps because of some variation of the impurity surface fluctuations) but it is independent of temperature. Note that the precise determination of radius dependence of C_d would require even further numerical simulations of what has been presented here.

In the inset of Fig. 7, we show the temperature dependence of the averaged excitations velocity (21), which turns out to be larger than the speed of phonons because it is dominated by high wave-number excitations. Note that the friction increment starts to diverge from the prediction at high temperatures. One reason is that the mean-free path of the GP excitations is becoming of the same order of the impurity size and thus the viscosity starts to play a role in the momentum exchange. A second cause may be that the impurity-excitations interactions are modified because of the high nonlinearity of the GP waves, leading to a temperature dependence of the constant C_d in Eq. (20). Eventually, note that a larger discordance with the measurements at high temperature is observed if the normal fluid density is used. This is probably

due to a lack of accuracy in the computation of ρ_n at high temperatures, but it also suggests that it can be more reasonable to identify the density of the excitations simply with that of the noncondensed modes.

IV. DISCUSSION

In this paper we studied how the stochastic motion of an active, finite-size, and immiscible impurity immersed in a GP quantum fluid changes when the temperature is varied. We demonstrated that the interaction with the thermal excitations in the system always leads to a fast thermalization of the impurity. At time lags larger than $10\xi/c$ the correlation function of the impurity velocity shows an exponential decay, which is steeper for higher temperatures. This and the impurity squared displacement are reminiscent of an Ornstein-Uhlenbeck process.

From the measurements of the velocity correlation we extracted the temperature dependence of the friction coefficient $\gamma(T)$. The clear result is that the impurity does not experience the typical Stokes drag present in a classical fluid. Indeed, in the case of Stokes drag, the temperature dependence of the friction (19) is through the viscosity η. Since the viscosity has been shown to be slightly decreasing with temperature in the FTGP model [35], it cannot explain the trend observed in Fig. 7. The reason is that the settings studied are associated with large values of the Knudsen number, meaning that at the scale of the impurity the GP quantum fluid at finite temperature cannot be considered as a continuous liquid. On the contrary, describing phenomenologically the system as a gas of dilute thermal excitations reproduces the correct temperature increment of the friction $\gamma(T)$. Moreover, we observe a dependence of the friction with the impurity size compatible with the quadratic scaling $\gamma \propto a_I^2$ predicted by the Epstein drag (20), despite some small deviations hidden in the prefactor C_d. In the case of Stokes drag, one should have observed a linear scaling $\gamma \propto a_I$ that is not in agreement with our data.

We stress that the picture outlined does not apply to the particles typically used as probes in superfluid helium experiments [15,16]. Indeed, aside from being liquid helium a strongly interacting system, the typical size of those particles is four orders of magnitude larger than the healing length. Thus, in that case the Knudsen number is certainly small enough to entail the standard Stokes drag. However, a similar regime in terms of Knudsen number has been studied experimentally by using microspheres in liquid helium below 0.5 K [53]. It has been observed that the drag is determined by the ballistic scattering of quasiparticles and the temperature dependence of the friction coefficient is given by the temperature dependence of the quasiparticles density. Aside from helium, we hope that our study may be relevant for future BEC experiments, in which finite-size and immiscible impurities can be produced in the strong repulsive regime of multicomponent condensates [22], or in the study of the impurity dynamics in quantum fluids of light [19,20].

A possible follow-on of this work is the development of a self-consistent theory for the interaction between the thermal excitations and the impurity, which takes into account the dependence on the wave numbers of the colliding waves. This

could give an analytical explanation to the small value of the prefactor C_d in Eq. (20) compared to the classical Epstein drag for elastic collisions. Note that in a recent publication, the motion of a bright soliton moving in a thermal cloud of distinct atoms has been successfully modeled by using an OU dynamics [54]. In that case, the soliton is treated by using a wave function and the thermal (noncondensed) cloud as a reservoir. Although in our model the impurity is a rigid body with classical degrees of freedom, the result of [54] could inspire an analytical derivation of the OU dynamics for an impurity [14]. Moreover, the characterization of the motion of a multitude of impurities in the FTGP system can be deepened, expanding the findings of Ref. [14]. Finally, the fundamental problem of vortex nucleation due to fast impurities has been thoroughly investigated at zero temperature [11–13], but few results are known in the finite-temperature regime [55,56].

In particular, the FTGP model coupled with impurities (1) would be a suitable framework to address the impurity-vortex interaction at nonzero temperature.

[1] L. Pitaevskii and S. Stringari, *Bose-Einstein Condensation and Superfluidity*, International Series of Monographs on Physics (Oxford University Press, Oxford, 2016).

[2] M. H. Anderson, J. R. Ensher, M. R. Matthews, C. E. Wieman, and E. A. Cornell, Observation of Bose-Einstein condensation in a dilute atomic vapor, Science **269**, 198 (1995).

[3] J. Kasprzak, M. Richard, S. Kundermann, A. Baas, P. Jeambrun, J. Keeling, F. Marchetti, M. Szymańska, R. Andre, J. Staehli *et al.*, Bose-Einstein condensation of exciton polaritons, Nature (London) **443**, 409 (2006).

[4] S. Demokritov, V. Demidov, O. Dzyapko, G. Melkov, A. Serga, B. Hillebrands, and A. Slavin, Bose-Einstein condensation of quasi-equilibrium magnons at room temperature under pumping, Nature (London) **443**, 430 (2006).

[5] J. Klaers, J. Schmitt, F. Vewinger, and M. Weitz, Bose–einstein condensation of photons in an optical microcavity, Nature (London) **468**, 545 (2010).

[6] P. Kapitza, Viscosity of Liquid Helium below the λ-Point, Nature (London) **141**, 74 (1938).

[7] J. F. Allen and A. D. Misener, Flow of Liquid Helium II, Nature (London) **141**, 75 (1938).

[8] I. Carusotto and C. Ciuti, Quantum fluids of light, Rev. Mod. Phys. **85**, 299 (2013).

[9] C. Nore, M. Abid, and M. E. Brachet, Decaying kolmogorov turbulence in a model of superflow, Phys. Fluids **9**, 2644 (1997).

[10] R. J. Donnelly, *Quantized Vortices in Helium II*, Vol. 2 (Cambridge University Press, Cambridge, 1991).

[11] T. Frisch, Y. Pomeau, and S. Rica, Transition to Dissipation in a Model of Superflow, Phys. Rev. Lett. **69**, 1644 (1992).

[12] C. Nore, C. Huepe, and M. E. Brachet, Subcritical Dissipation in Three-Dimensional Superflows, Phys. Rev. Lett. **84**, 2191 (2000).

[13] T. Winiecki and C. S. Adams, Motion of an object through a quantum fluid, Europhys. Lett. **52**, 257 (2000).

[14] U. Giuriato, G. Krstulovic, and D. Proment, Clustering and phase transitions in a 2d superfluid with immiscible active impurities, J. Phys. A: Math. Theor. **52**, 305501 (2019).

[15] G. P. Bewley, D. P. Lathrop, and K. R. Sreenivasan, Superfluid helium: Visualization of quantized vortices, Nature (London) **441**, 588 (2006).

[16] M. La Mantia and L. Skrbek, Quantum turbulence visualized by particle dynamics, Phys. Rev. B **90**, 014519 (2014).

[17] N. Spethmann, F. Kindermann, S. John, C. Weber, D. Meschede, and A. Widera, Dynamics of Single Neutral Impurity Atoms Immersed in an Ultracold Gas, Phys. Rev. Lett. **109**, 235301 (2012).

[18] M. Hohmann, F. Kindermann, T. Lausch, D. Mayer, F. Schmidt, E. Lutz, and A. Widera, Individual Tracer Atoms in an Ultracold Dilute Gas, Phys. Rev. Lett. **118**, 263401 (2017).

[19] C. Michel, O. Boughdad, M. Albert, P.-É. Larré, and M. Bellec, Superfluid motion and drag-force cancellation in a fluid of light, Nat. Commun. **9**, 2108 (2018).

[20] I. Carusotto, Superfluid light in bulk nonlinear media, Proc. R. Soc. A **470**, 20140320 (2014).

[21] P. G. Kevrekidis, D. J. Frantzeskakis, and R. Carretero-González, *Emergent Nonlinear Phenomena in Bose-Einstein Condensates*, Vol. 45 (Springer, Berlin, 2008).

[22] S. Rica and D. C. Roberts, Induced interaction and crystallization of self-localized impurity fields in a bose-einstein condensate, Phys. Rev. A **80**, 013609 (2009).

[23] G. Modugno, M. Modugno, F. Riboli, G. Roati, and M. Inguscio, Two Atomic Species Superfluid, Phys. Rev. Lett. **89**, 190404 (2002).

[24] C. J. Myatt, E. A. Burt, R. W. Ghrist, E. A. Cornell, and C. E. Wieman, Production of Two Overlapping Bose-Einstein Condensates by Sympathetic Cooling, Phys. Rev. Lett. **78**, 586 (1997).

[25] S. B. Papp, J. M. Pino, and C. E. Wieman, Tunable Miscibility in a Dual-Species Bose-Einstein Condensate, Phys. Rev. Lett. **101**, 040402 (2008).

[26] N. P. Proukakis and B. Jackson, Finite-temperature models of bose–einstein condensation, J. Phys. B: At., Mol. Opt. Phys. **41**, 203002 (2008).

[27] E. Zaremba, T. Nikuni, and A. Griffin, Dynamics of trapped bose gases at finite temperatures, J. Low Temp. Phys. **116**, 277 (1999).

[28] M. J. Davis, S. A. Morgan, and K. Burnett, Simulations of Bose Fields at Finite Temperature, Phys. Rev. Lett. **87**, 160402 (2001).

[29] S. Nazarenko, M. Onorato, and D. Proment, Bose-einstein condensation and berezinskii-kosterlitz-thouless transition in the two-dimensional nonlinear schrödinger model, Phys. Rev. A **90**, 013624 (2014).

[30] C. Connaughton, C. Josserand, A. Picozzi, Y. Pomeau, and S. Rica, Condensation of Classical Nonlinear Waves, Phys. Rev. Lett. **95**, 263901 (2005).

[31] G. Krstulovic and M. Brachet, Dispersive Bottleneck Delaying Thermalization of Turbulent Bose-Einstein Condensates, Phys. Rev. Lett. **106**, 115303 (2011).

[32] N. G. Berloff and A. J. Youd, Dissipative Dynamics of Superfluid Vortices at Nonzero Temperatures, Phys. Rev. Lett. **99**, 145301 (2007).

[33] G. Krstulovic and M. Brachet, Anomalous vortex-ring velocities induced by thermally excited kelvin waves and counterflow effects in superfluids, Phys. Rev. B **83**, 132506 (2011).

[34] G. Krstulovic and M. Brachet, Energy cascade with small-scale thermalization, counterflow metastability, and anomalous velocity of vortex rings in fourier-truncated gross-pitaevskii equation, Phys. Rev. E **83**, 066311 (2011).

[35] V. Shukla, P. D. Mininni, G. Krstulovic, P. C. di Leoni, and M. E. Brachet, Quantitative estimation of effective viscosity in quantum turbulence, Phys. Rev. A **99**, 043605 (2019).

[36] V. Shukla, R. Pandit, and M. Brachet, Particles and fields in superfluids: Insights from the two-dimensional gross-pitaevskii equation, Phys. Rev. A **97**, 013627 (2018).

[37] U. Giuriato and G. Krstulovic, Interaction between active particles and quantum vortices leading to kelvin wave generation, Sci. Rep. **9**, 4839 (2019).

[38] U. Giuriato, G. Krstulovic, and S. Nazarenko, How trapped particles interact with and sample superfluid vortex excitations, Phys. Rev. Research **2**, 023149 (2020).

[39] U. Giuriato and G. Krstulovic, Quantum vortex reconnections mediated by trapped particles, Phys. Rev. B **102**, 094508 (2020).

[40] U. Giuriato and G. Krstulovic, Active and finite-size particles in decaying quantum turbulence at low temperature, Phys. Rev. Fluids **5**, 054608 (2020).

[41] N. G. Berloff and P. H. Roberts, Motion in a bose condensate: VIII. the electron bubble, J. Phys. A: Math. Gen. **34**, 81 (2000).

[42] A. Villois and H. Salman, Vortex nucleation limited mobility of free electron bubbles in the gross-pitaevskii model of a superfluid, Phys. Rev. B **97**, 094507 (2018).

[43] J. Rønning, A. Skaugen, E. Hernández-García, C. Lopez, and L. Angheluta, Classical analogies for the force acting on an impurity in a bose–einstein condensate, New J. Phys. **22**, 073018 (2020).

[44] G. E. Astrakharchik and L. P. Pitaevskii, Motion of a heavy impurity through a bose-einstein condensate, Phys. Rev. A **70**, 013608 (2004).

[45] T. Lee, On some statistical properties of hydrodynamical and magneto-hydrodynamical fields, Q. Appl. Math. **10**, 69 (1952).

[46] R. H. Kraichnan, Inertial ranges in two-dimensional turbulence, The Physics of Fluids **10**, 1417 (1967).

[47] R. Clark and G. Derrick, *Mathematical Methods in Solid State and Superfluid Theory: Scottish Universities? Summer School*, Scottish Universities' Summer School (Springer, New York, 1968).

[48] C. J. Foster, P. B. Blakie, and M. J. Davis, Vortex pairing in two-dimensional Bose gases, Phys. Rev. A **81**, 023623 (2010).

[49] N. G. Van Kampen, *Stochastic Processes in Physics and Chemistry*, Vol. 1 (Elsevier, Amsterdam, 1992).

[50] C. K. Batchelor and G. Batchelor, *An Introduction to Fluid Dynamics* (Cambridge University Press, Cambridge, 2000).

[51] P. S. Epstein, On the resistance experienced by spheres in their motion through gases, Phys. Rev. **23**, 710 (1924).

[52] B. de Lima Bernardo, F. Moraes, and A. Rosas, Drag force experienced by a body moving through a rarefied gas, Chin. J. Phys. **51**, 189 (2013).

[53] M. Niemetz and W. Schoepe, Stability of laminar and turbulent flow of superfluid 4he at mk temperatures around an oscillating microsphere, J. Low Temp. Phys. **135**, 447 (2004).

[54] R. G. McDonald and A. S. Bradley, Brownian motion of a matter-wave bright soliton moving through a thermal cloud of distinct atoms, Phys. Rev. A **93**, 063604 (2016).

[55] M. Leadbeater, T. Winiecki, and C. S. Adams, Effect of condensate depletion on the critical velocity for vortex nucleation in quantum fluids, J. Phys. B: At., Mol. Opt. Phys. **36**, L143 (2003).

[56] G. W. Stagg, R. W. Pattinson, C. F. Barenghi, and N. G. Parker, Critical velocity for vortex nucleation in a finite-temperature bose gas, Phys. Rev. A **93**, 023640 (2016).